Electronic Supplementary Material (ESI) for Journal of Materials Chemistry

Supporting Information

Conducting and Ordered Carbon Films Obtained by Pyrolysis of Covalently Attached Polyphenylene and Polyanthracene Layers on Silicon Substrates

Kristian Torbensen,[†] Joseph Iruthayaraj,[†,‡] Marcel Ceccato,[†] Mikkel Kongsfelt,[†]

Thomas Breitenbach,[†,#] Steen Uttrup Pedersen,[†,‡] and Kim Daasbjerg[†,‡]

[†] *Department of Chemistry, Aarhus University, Langelandsgade 140, DK-8000 Aarhus, Denmark*

[‡] *Interdisciplinary Nanoscience Center (iNANO), Department of Physics and Astronomy, Aarhus University, Ny Munkegade 120, DK-8000 Aarhus C, Denmark*

[#] *Center of Oxygen Microscopy and Imaging (COMI), Department of Chemistry, Aarhus University, Langelandsgade 140, DK-8000 Aarhus, Denmark.*

Electrografting of anthracene-9-diazonium (AD) tetrafluoroborate on SiH. Figure S1 shows voltammograms pertaining to the grafting of AD in MeCN in absence of supporting electrolyte. The first voltammetric sweep exhibits a broad and ill-defined reduction peak. The second cycle shows a considerable decrease of the faradaic current and the same is even to a larger extent seen for the third cycle recorded after having carried out a potentiostatic electrolysis at –1.87 V vs SCE for 300 s. This indicates that the grafting process, no matter if it is carried out by cyclic voltammetry or electrolysis, results in the formation of an insulating film on the substrate.

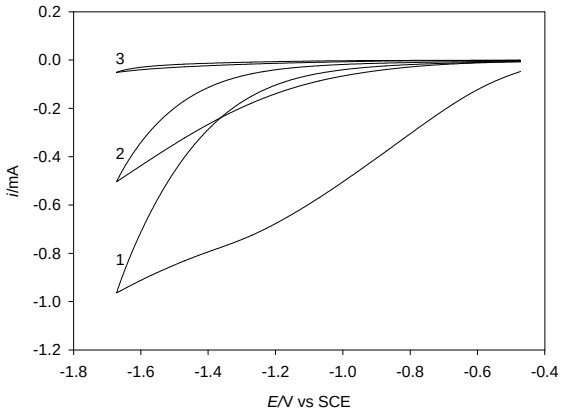

Figure S1. Cyclic voltammograms of 8 mM AD recorded at a freshly prepared SiH substrate using $v = 0.1$ V s^{-1} in MeCN before (cycles 1 and 2) and after (cycle 3) a potentiostatic electrolysis performed at –1.87 V vs SCE for 300 s in MeCN.

Electrochemical characterization of SiH_{PA} and SiH-PGF_{PA}. Figure S2 shows cyclic voltammograms recorded of the redox probe, $K_3Fe(CN)_6$, at SiH_{PA} and Si-PGF_{PA}. The voltammograms are similar to those recorded at the SiH_{PP} and SiH-PGF_{PP} substrates, in that the modified substrate before pyrolysis is strongly blocking, while after pyrolysis a quasi-reversible electron transfer is observed. This indicates that the pyrolysis process promotes the formation of a conducting carbon film.

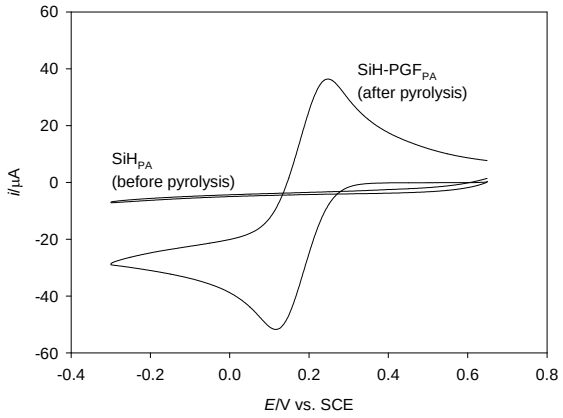

Figure S2. Cyclic voltammograms of 1 mM $K_3Fe(CN)_6$ recorded at SiH_{PA} and $SiH\text{-}PGF_{PA}$ using v = 0.1 V s^{-1} in 0.1 M KCl pH 7 phosphate buffered solution. Electrical contact to the PGF was made through the silicon substrate.

Thickness of the grafted pyrolyzed films. Since the ellipsometric data for the SiH substrate changed significantly during the pyrolysis process, the thickness of the SiH-PGFs was assumed to be the same as estimated from the shrinkage of the corresponding films that had been grafted and subsequently pyrolyzed directly on the native SiO_2/Si substrate (denoted Si-PGF). Figure S3 shows the thickness of these pyrolyzed films plotted against the thickness of the grafted films. The slope of the straight line obtained by linear regression corresponds to the fraction of material remaining in the film after pyrolysis, hence revealing that the shrinkage in percentage constitutes 33% and 16% for $Si\text{-}PGF_{PP}$ and $Si\text{-}PGF_{PA}$, respectively.

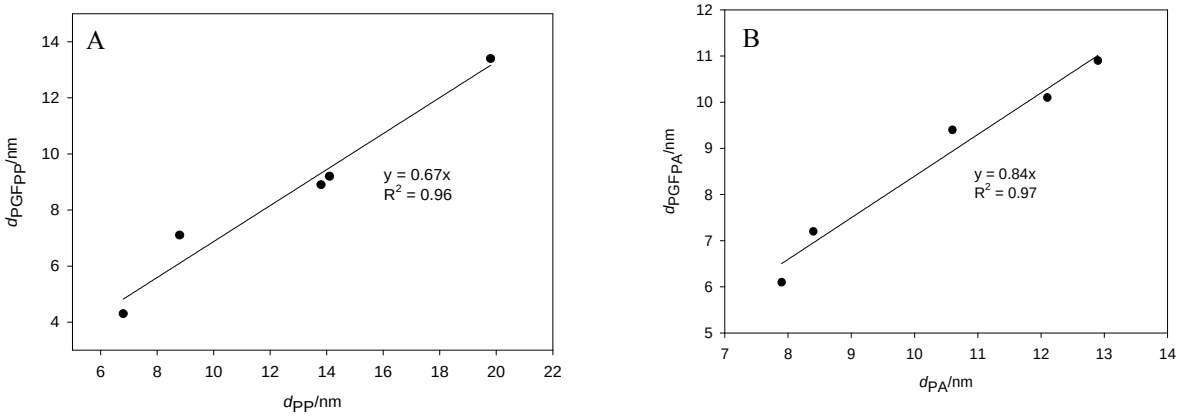

Figure S3. Plot of the thickness of pyrolyzed films ($d_{PGF_{PP}}$ or $d_{PGF_{PA}}$) vs the thickness of grafted films (d_{PP} or d_{PA}) of (A) polyphenylene and (B) polyanthracene on SiO_2/Si substrate.

Determination of k^0 of redox probes at GC, PPF, and PGF substrates. In a series of experiments k^0 was determined for three redox probe systems, i.e. $K_3Fe(CN)_6$ and $Ru(NH_3)_6Cl_3$ in pH 7 phosphate buffer (2.59×10^{-2} M KH_2PO_4 + 4.61×10^{-2} M Na_2HPO_4)/0.1 M KCl, and ferrocene in 0.1 M Bu_4NBF_4/MeCN by evaluating the development in ΔE_p as a function of the sweep rate, v. In general, for the quasi-reversible systems mentioned above, the rate determining step is governed by the heterogeneous charge transfer comprised by k^0. As v is increased, the experimental time scale is shortened and higher overpotentials, reflected by an increase in ΔE_p, is required in order for the system to maintain equilibrium. By calculating ψ defined as $(-0.6288 + 0.0021n\Delta E_p)/(1 - 0.017n\Delta E_p)$ for $\Delta E_p < 0.15$ V or $2.18(\alpha/\pi)^{1/2}\exp[-(\alpha^2F/RT)n\Delta E_p]$ for $\Delta E_p > 0.15$ V, k^o could be determined as the slope of the plot of ψ vs $(\pi DnF/RT)^{-1/2}v^{-1/2}$, where D denotes the diffusion coefficient of the electroactive species, n the number of electrons involved in the electrochemical process, and F Faraday constant.[S1] The value of n was set to 1 for all species and $D = 0.6 \times 10^{-5}$, 0.6×10^{-5}, and 2.4×10^{-5} cm^2 s^{-1} for $Fe(CN)_6^{3-/4-}$, $Ru(NH_3)_6^{3+/2+}$, and $Fc^{+/0}$, respectively.[S2-S4] All redox systems were treated using classical Butler-Volmer theory, in which the charge transfer coefficient α is considered to be constant, i.e. independent of the applied potential. In this work α was set to 0.5 to be in accordance with literature results.

Figures S4–S9 show the plots of ψ as a function of v with the electrochemical data obtained at SiH-PGF_{PP}, SiH-PGF_{PA}, Si-PPF, GC, Si-PGF_{PP} and Si-PGF_{PA}, respectively, where "Si" refers to a SiO_2/Si surface.

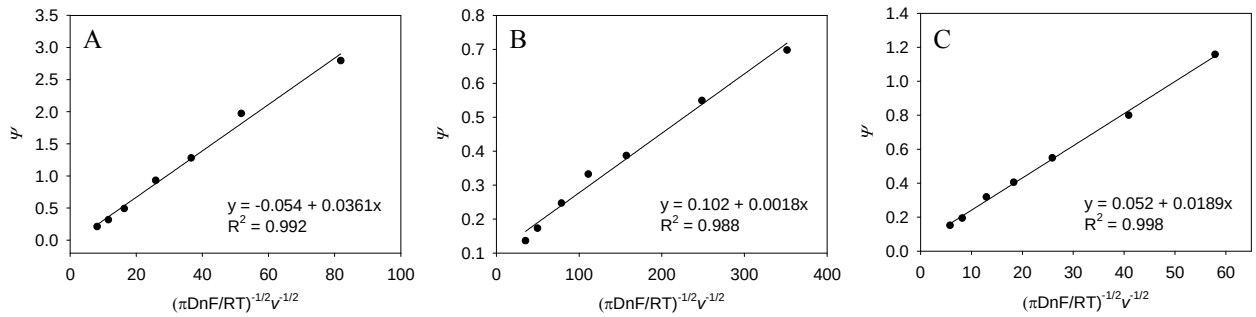

Figure S4. Plot of ψ vs $(\pi DnF/RT)^{-1/2}v^{-1/2}$ at SiH-PGF_{PP} for (A) $Ru(NH_3)_6Cl_3$, (B) $K_3Fe(CN)_6$, and (C) ferrocene.

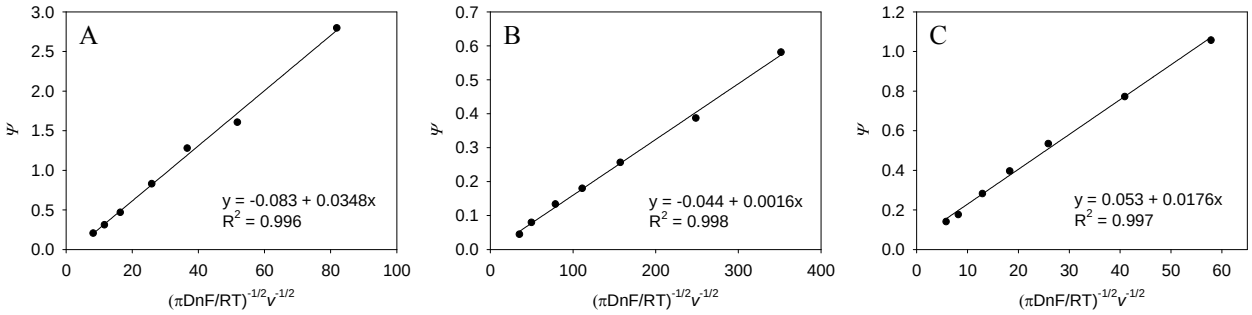

Figure S5. Plot of ψ vs $(\pi DnF/RT)^{-1/2}v^{-1/2}$ at SiH-PGF_{PA} for (A) $Ru(NH_3)_6Cl_3$, (B) $K_3Fe(CN)_6$, and (C) ferrocene.

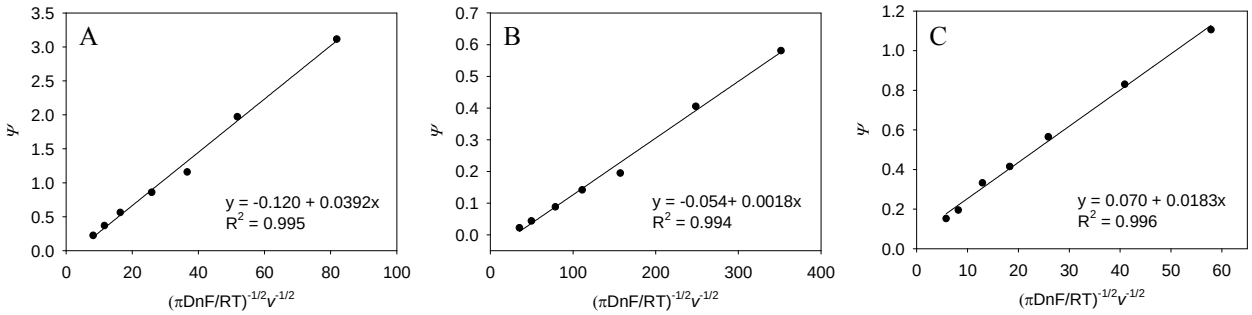

Figure S6. Plot of ψ vs $(\pi DnF/RT)^{-1/2}v^{-1/2}$ at Si-PPF for (A) $Ru(NH_3)_6Cl_3$, (B) $K_3Fe(CN)_6$, and (C) ferrocene.

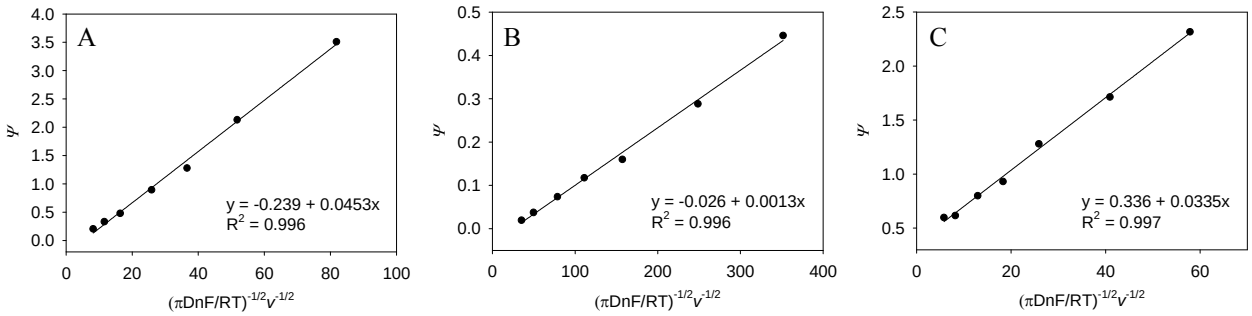

Figure S7. Plot of ψ vs $(\pi DnF/RT)^{-1/2}v^{-1/2}$ at GC for (A) $Ru(NH_3)_6Cl_3$, (B) $K_3Fe(CN)_6$, and (C) ferrocene.

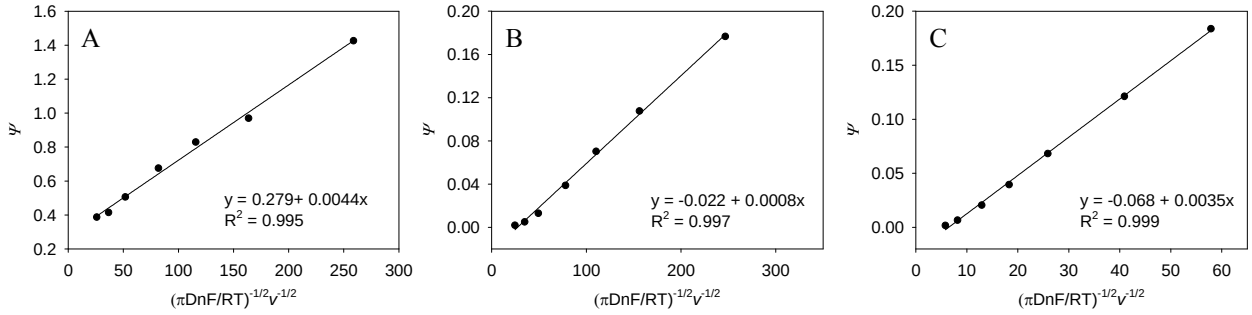

Figure S8. Plot of ψ vs $(\pi DnF/RT)^{-1/2}v^{-1/2}$ at Si-PGF_{PP} for (A) $Ru(NH_3)_6Cl_3$, (B) $K_3Fe(CN)_6$, and (C) ferrocene.

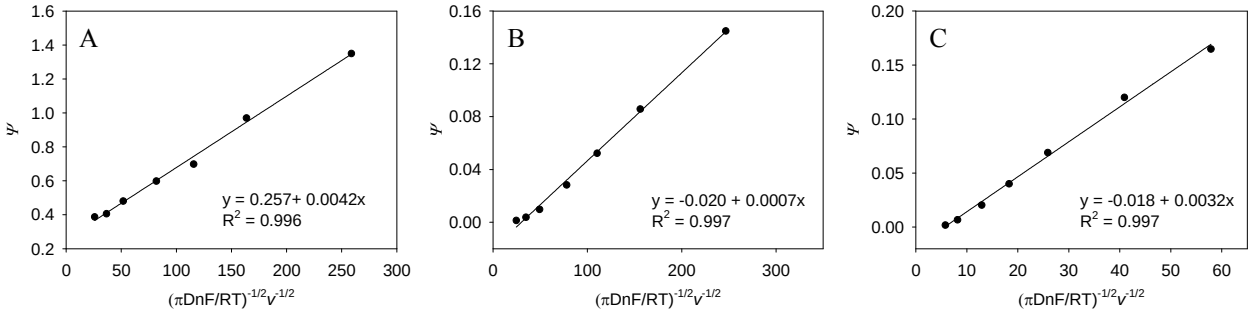

Figure S9. Plot of ψ vs $(\pi DnF/RT)^{-1/2}v^{-1/2}$ at Si-PGF_{PA} for (A) $Ru(NH_3)_6Cl_3$, (B) $K_3Fe(CN)_6$, and (C) ferrocene.

Table S1 shows the values of k^0 for the PGFs formed on native SiO_2/Si substrates. Compared with the corresponding results obtained for the SiH substrates, the k^0 values are diminished by factors of 2, 5, and 8 for $K_3Fe(CN)_6$, $Ru(NH_3)_6Cl_3$, and ferrocene, respectively. This lowering of k^0 can be attributed to the effect from the insulating character of the upper SiO_2 layer ($d_{SiO_2} \approx 3$ nm).

Table S1. Values of k^0 Determined for the Redox Couples $Ru(NH_3)_6^{3+/2+}$, $Fe(CN)_6^{3-/4-}$, and $Fc^{+/0}$ at Si-PGF_{PP} and Si-PGF_{PA}.

Carbon film	Substrate	d (nm)	$Ru(NH_3)_6^{3+/2+}$ 10^3k^0 (cm s^{-1})	$Fe(CN)_6^{3-/4-}$ 10^3k^0 (cm s^{-1})	$Fc^{0/+}$ 10^3k^0 (cm s^{-1})
PGF_{PP}	SiO_2/Si	7.1 ± 0.5	4.4	0.8	3.5
PGF_{PA}	SiO_2/Si	7.2 ± 0.4	4.2	0.7	3.2

Characterization of the SiH-PGF$_{PP}$ substrate by XPS. From high resolution XPS spectra of SiH-PGF$_{PP}$ six different types of carbon in C1s and three types of oxygen in O1s regions were identified in accordance with the fitting results presented in Figure S10A,B.

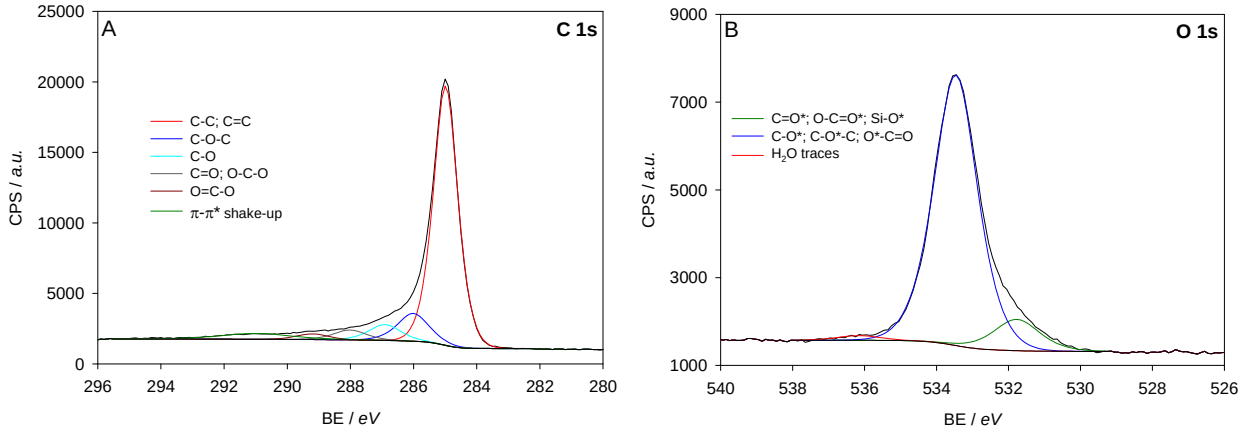

Figure S10. High resolution XPS spectra (A) C 1s and (B) O 1s of SiH-PGF$_{PP}$.

From C 1s high resolution spectrum it is possible to identify a peak at 285.0 eV corresponding to the sp^2 and sp^3 hybridized C-C bonds. The component at 286.0 eV is assigned to C-O-C groups and the peak at a binding energy of 286.9 eV originates from C-O groups. The peaks at 288.0 eV and 289.2 eV are ascribed to C=O and O=C-O groups, respectively, while the last peak at 291.0 eV is recognized as "shake-up satellites" originating from the bonding to anti-bonding transition of the π molecular orbital.

The O 1s high resolution spectrum was deconvoluted into three peaks. The peak at 531.7 eV is ascribed to C=O and Si-O groups while the peak at 533.4 eV originates from C-O groups. A third peak at 536.1 eV is needed for a good fit and is assigned to presence of water traces.

Electrografting of 4-nitrobenzenediazonium (NBD) tetrafluoroborate on SiH-PGF$_{PA}$ and PPF. Figure S11A,B shows voltammograms recorded of the grafting of NBD on SiH-PGF$_{PA}$ and PPF, respectively. In both cases a well-defined grafting peak is seen on the first voltammetric sweep, while the current decreases rapidly on the second and, in particular, the third cycle. The latter is obtained after electrolysis had been performed at –0.2 V vs SCE (200 mV negative to the peak potential) for 300 s. This behaviour is consistent with the formation of a grafted and insulating layer of 4-nitrophenyl groups.

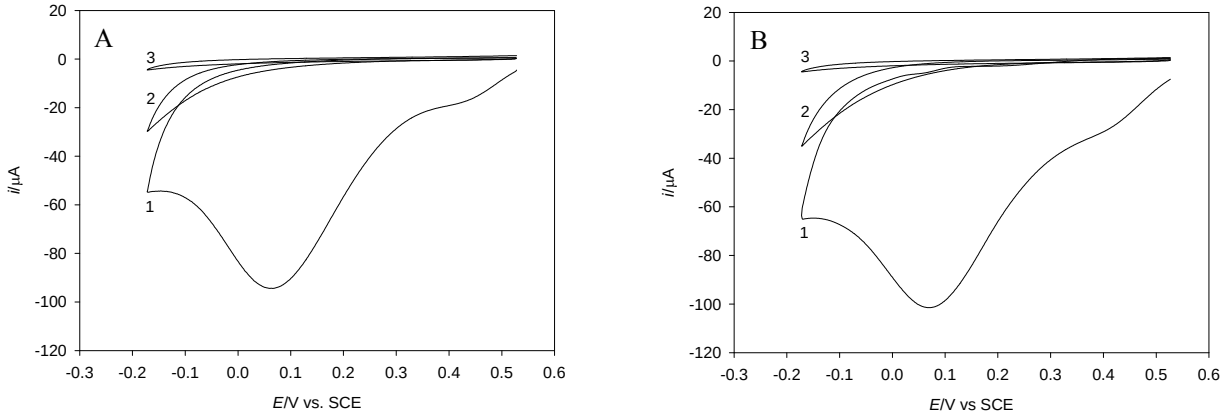

Figure S11. Cyclic voltammograms of 2 mM NBD recorded using v = 0.1 V s^{-1} in 0.1 M Bu_4NBF_4/MeCN at (A) SiH-PGF$_{PA}$ and (B) PPF (on a SiO_2/Si substrate) before (cycles 1 and 2) and after (cycle 3) a potentiostatic electrolysis performed at –1.87 V vs SCE for 300 s in MeCN.

Electrochemical characteristics of SiH-PGF$_{PA}^{NB}$ and PPF^{NB}. Figure S12A,B shows cyclic voltammetric responses of the PGF$_{PA}^{NB}$ and PPF^{NB} electrodes, respectively, in a blank 0.1 M Bu_4NBF_4/MeCN solution.

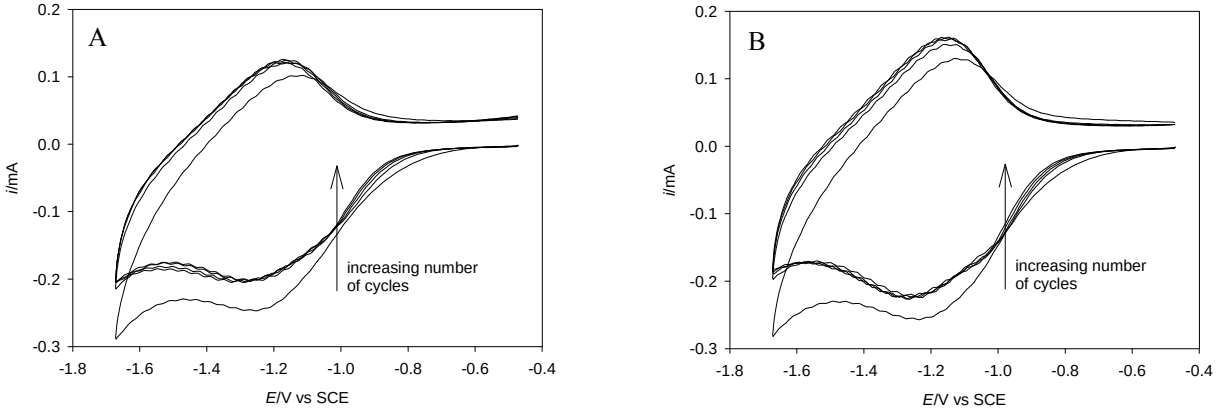

Figure S12. Cyclic voltammograms recorded at (A) SiH-PGF$_{PA}^{NB}$ and (B) Si-PPF^{NB} using v = 2 V s^{-1} in 0.1 M Bu_4NBF_4/MeCN.

AFM images of PPF and pyrolyzed grafted films on SiO_2/Si. Figure S13A,B shows AFM images of PPF before and after electrografting of NBD on SiO_2/Si, respectively.

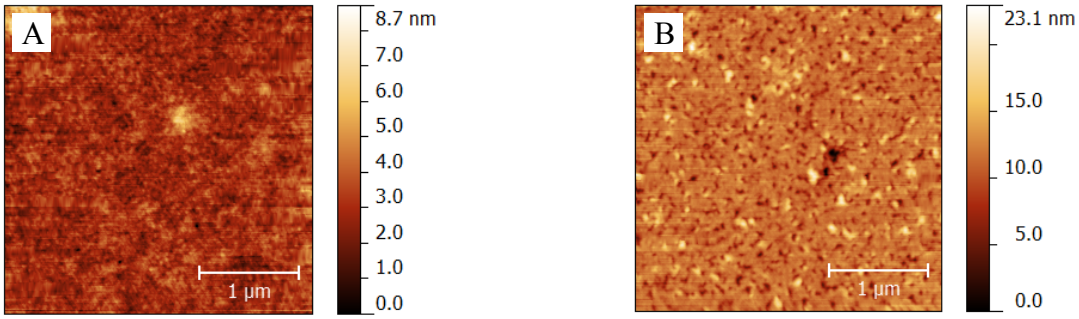

Figure S13. AFM non-contact tapping mode images of scan size 3 × 3 µm^2 for (A) Si-PPF (R_q = 0.6 ± 0.1 nm, d = 94.7 ± 0.2 nm) and (B) 4 nm thick NB film on Si-PPF^{NB} (R_q = 2.7 ± 0.1 nm).

Figure 14A,B shows AFM images of the PP film before and after pyrolysis at 1050 ºC for 30 min on SiO_2/Si (denoted Si_{PP}), respectively. The electrografting was carried out using BD as grafting agent in the same procedure as described for the H-terminated substrates. In general, thinner films were obtained at the SiO_2/Si substrates because of the insulating character of the upper SiO_2 layer.

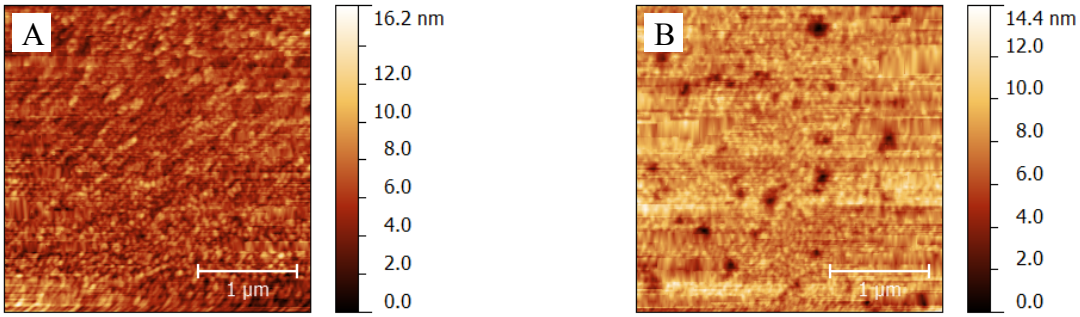

Figure S14. AFM non-contact tapping mode images of scan size 3 × 3 µm^2 for (A) Si_{PP} (R_q = 1.7 ± 0.1 nm, d = 20.6 ± 1.2 nm nm) and (B) Si-PGF_{PP} (R_q = 1.4 ± 0.1 nm, d = 13.4 ± 0.7 nm).

Figure 15A,B shows the AFM images for the corresponding Si_{PA} film.

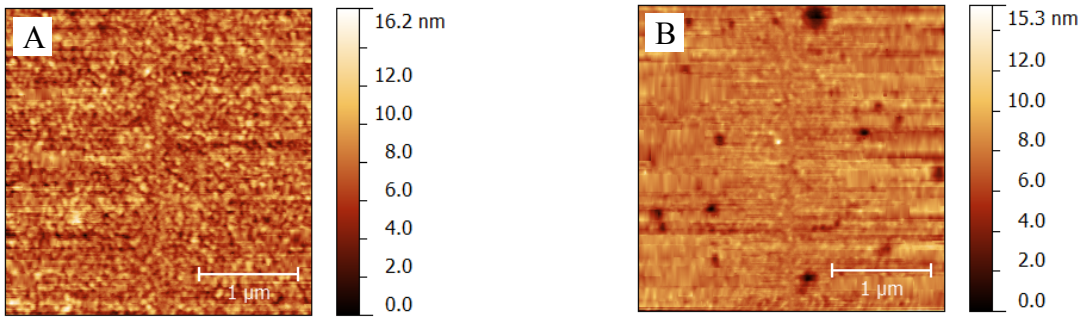

Figure S15. AFM non-contact tapping mode images of scan size 3 × 3 µm^2 for (A) Si_{PA} (R_q = 1.8 ± 0.1 nm, d = 13.4 ± 0.7 nm nm) and (B) Si-PGF_{PA} (R_q = 1.2 ± 0.1 nm, d = 10.9 ± 0.8 nm).

References

(S1) Lavagnini, I.; Antiochia, R.; Magno, F. *Electroanalysis* **2004**, *16*, 505–506.

(S2) Dumanlı, O.; Onar, A. N. *Electrochim. Acta* **2009**, *54*, 6438–6444.

(S3) Bilewicz, R.; Sawaguchi, T.; Chamberlain, R. V.; Majda, M. *Langmuir* **1995**, *11*, 2256–2266.

(S4) Jacob, S. R.; Hong, Q.; Coles, B. A.; Compton, R. G. *J. Phys. Chem. B* **1999**, *103*, 2963–2969.